



# CHORUS

This is the accepted manuscript made available via CHORUS. The article has been published as:

## Electron Trapping from Interactions between Laser-Driven Relativistic Plasma Waves

Grigory Golovin, Wenchao Yan, Ji Luo, Colton Fruhling, Dan Haden, Baozhen Zhao, Cheng Liu, Min Chen, Shouyuan Chen, Ping Zhang, Sudeep Banerjee, and Donald Umstadter

Phys. Rev. Lett. **121**, 104801 — Published 7 September 2018

DOI: [10.1103/PhysRevLett.121.104801](https://doi.org/10.1103/PhysRevLett.121.104801)

1 **Electron trapping from interactions between laser-driven relativistic plasma waves**

2 Grigory Golovin,<sup>1</sup> Wenchao Yan,<sup>1</sup> Ji Luo,<sup>2,3</sup> Colton Fruhling,<sup>1</sup> Dan Haden,<sup>1</sup> Baozhen Zhao,<sup>1</sup> Cheng Liu,<sup>1</sup>  
3 Min Chen,<sup>2,3</sup> Shouyuan Chen,<sup>1</sup> Ping Zhang,<sup>1</sup> Sudeep Banerjee,<sup>1</sup> and Donald Umstadter<sup>1</sup>

4 **Interactions of large-amplitude relativistic plasma waves were investigated experimentally by**  
5 **propagating two synchronized ultra-intense femtosecond laser pulses in plasma at oblique crossing**  
6 **angles to each other. The electrostatic and electromagnetic fields of the colliding waves acted to pre-**  
7 **accelerate and trap electrons via previously predicted, but untested injection mechanism of**  
8 **ponderomotive drift and wake-wake interference. High-quality energetic electron beams were**  
9 **produced, also revealing valuable new information about plasma-wave dynamics.**

10 Interactions between relativistic plasma waves are central to plasma physics, astrophysics [1,2],  
11 controlled fusion [3], wakefield electron accelerators [4--7], and compact x-ray sources [8,9]. Recently-  
12 developed capabilities – for driving relativistic transverse electromagnetic plasma waves (referred here  
13 simply as laser pulses), and relativistic longitudinal electrostatic wakefield electron plasma waves  
14 (referred here as wakes) – have greatly enhanced laboratory studies. The greatest current interest in these  
15 waves stems from their remarkably high acceleration gradients (TeV/cm and GeV/cm, respectively).  
16 Wakes can be driven either by short-duration laser or charged-particle pulses. Such wakes have been  
17 shown to accelerate electrons to  $> \text{GeV}$  energy in distances of just cm [10] or m [11], respectively.  
18 However, for electrons to gain energy from the wake, they must first become trapped by it.

19 A force must be exerted on an electron to give it the velocity and phase required for trapping, i.e., inject it  
20 into the wake. In the case of plasma-based electron accelerators, since the phase velocity of the wake is  
21 relativistic, so too is the velocity required for injection. Several mechanisms can be employed to provide  
22 the injection force. A propagating wake can self-inject, such as when it breaks [12], or when its  
23 wavelength suddenly changes due to defocusing of the wake driver [13], or due to an encounter with a  
24 sharp plasma-density gradient [14--16]. Alternatively, the wake driver can liberate and inject new  
25 electrons via photo-ionization [17,18].

26 The greatest flexibility and control over the injection process can be achieved when the injector is  
27 separate from the wake driver. In this case, the phase of the wake into which the electrons are injected can  
28 be precisely controlled, resulting in improved accelerator performance with reduced energy spread and

---

<sup>1</sup> Department of Physics and Astronomy, University of Nebraska-Lincoln, Lincoln, Nebraska 68588, USA

<sup>2</sup> Key Laboratory for Laser Plasmas (Ministry of Education) and School of Physics and Astronomy, Shanghai Jiao  
Tong University, Shanghai 200240, China

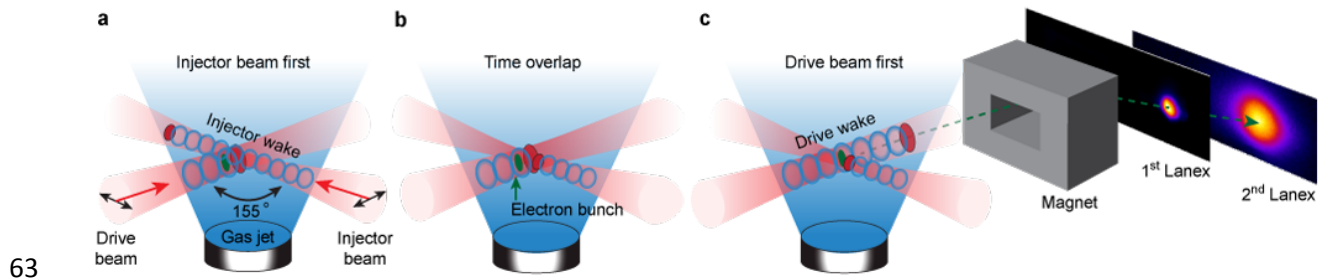
<sup>3</sup> Collaborative Innovation Center of IFSA (CICIFSA), Shanghai Jiao Tong University, Shanghai 200240, China

29 beam emittance. If an intense laser pulse is used as the injector (referred as optical injection), it can inject  
30 electrons via a time-averaged ponderomotive drift in its steep electromagnetic field gradient [19], photo-  
31 ionization [19--21], or stochastic heating in an optical beatwave [22--29]. Injection can be also caused by  
32 interference of overlapping wakes [30--32].

33 Reported here is the first experimental demonstration of two of these controlled injection mechanisms:  
34 ponderomotive drift and wake-wake interference, both of which had originally been proposed  
35 theoretically more than two decades ago [19,30]. Two laser pulses (drive and injector) were propagated  
36 through plasma obliquely and in crossing directions. Both were focused to sufficiently high intensity  
37 levels to drive their own wakes, enabling injection by wake-wake interference. The intensity of the  
38 injector pulse ( $1.7 \times 10^{20} \text{ W/cm}^2$ ) was several orders of magnitude higher than what was used in prior  
39 experiments on beatwave injection [23--29], high enough to cause injection via ponderomotive drift. To  
40 eliminate contribution from the competing mechanism of beatwave injection, the delay between when the  
41 drive and injector pulses arrived at their intersection was varied over a large range. Injection was  
42 observed by measuring the properties of the e-beams accelerated in the drive pulse direction. The  
43 dependence of these properties on the delay also proved to be a novel diagnostic of wake period and  
44 lifetime.

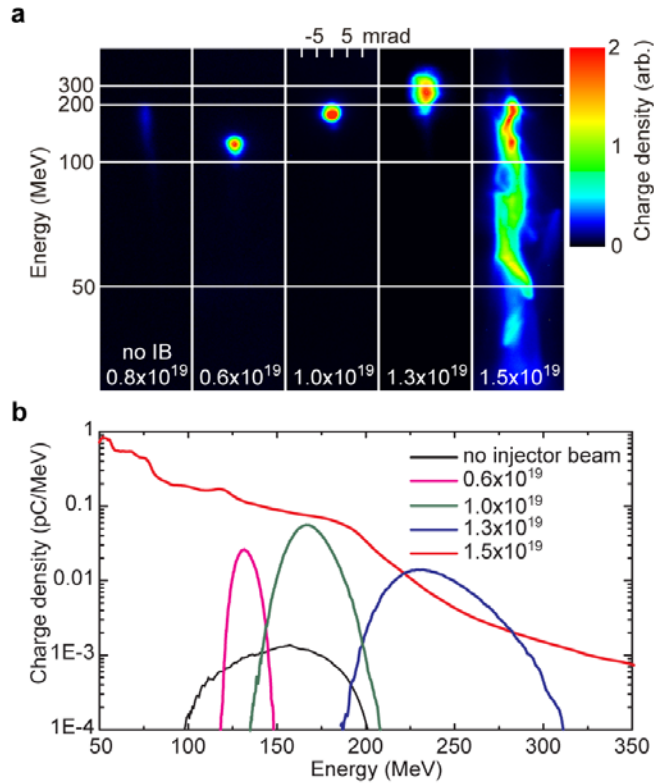
45 The experiments were performed at the Extreme Light Laboratory, University of Nebraska-Lincoln [33].  
46 After amplification, the laser pulse (800 nm, oscillation period of 2.67 fs) was split into two pulses, which  
47 were compressed by independent grating compressors [34]. An  $f/14$  parabolic mirror focused the drive  
48 pulse (1.2 J, 36 fs) to a 20- $\mu\text{m}$  (FWHM) focal spot, corresponding to normalized vector potential of  
49  $a_0 = 1.4$ . An  $f/2$  parabolic mirror focused the injector pulse (0.9 J, 34 fs) to a 2.8- $\mu\text{m}$  focal spot,  
50 corresponding to intensity of  $1.7 \times 10^{20} \text{ W/cm}^2$  ( $a_0 \sim 9$ ). We chose the tight focusing geometry to  
51 maximize the injector pulse intensity and access the regime of ponderomotive drift and wake-wake  
52 interference injection. Adaptive closed-loop feedback-control systems corrected the spectral phase  
53 distortions [35] and spatial aberrations [36] of both pulses. The pulses were polarized in the horizontal  
54 plane and intersected at an oblique angle ( $155^\circ$ ) inside a 2-mm gas jet [37]. Because the ponderomotive  
55 force of the injector pulse and the wakefields of the drive pulse are both three-dimensional, having  
56 comparable longitudinal and transverse components, electrons can be kicked into many different angles  
57 and subsequently trapped [19,39]. Thus, the injection mechanisms under study are expected to occur for a  
58 wide range of interaction angles. Although it may not have been optimal, the choice of interaction angle  
59 used in this experiment was based on the sizes of available optics and working space. An optical delay  
60 line adjusted the arrival times of the pulses to their intersection. The e-beam energy spectra were

61 measured using a double-screen (fast Lanex) magnetic spectrometer (0.7-T, 15-cm-long magnet) with 1%  
62 energy resolution for 100-300 MeV.



64 Figure 1. Schematic of the experiment. By changing the delay between pulse arrival times, three scenarios  
65 resulted: a) the drive pulse arrives at the intersection after the injector one and interacts with the injector  
66 wake. b) Both pulses arrive at the intersection simultaneously. c) The injector pulse arrives at the  
67 intersection after the drive one and interacts with the drive wake. The polarization of the laser pulses is  
68 horizontal (black arrows), with the directions indicated by red arrows.

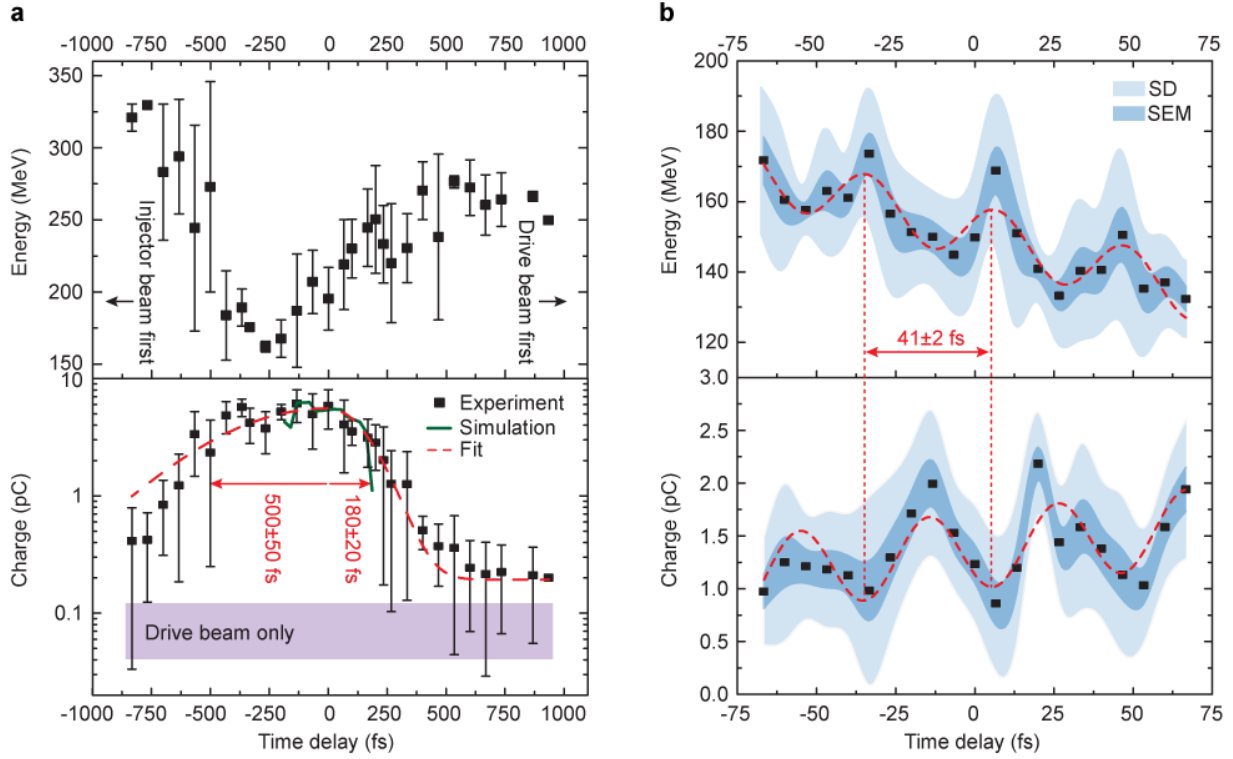
69 We started with the laser pulses overlapped in time (Figure 1b). In this scenario, we observed stable,  
70 quasi-monoenergetic (4% RMS spread), few-pC e-beams. By varying the plasma density over  
71  $(0.65 - 1.30) \times 10^{19} \text{ cm}^{-3}$ , the e-beams were tuned from 130-170 MeV. With the drive pulse alone, we  
72 observed stable, quasi-monoenergetic ( $\sim 10\%$  RMS) e-beams, but with two orders of magnitude lower  
73 charge ( $80 \pm 40 \text{ fC}$  based on 20 shots averaging). This single-pulse self-injection is likely due to marginal  
74 wave-breaking over a short distance. Massive continuous self-injection occurred at higher densities (  
75  $> 1.30 \times 10^{19} \text{ cm}^{-3}$ ) for both cases: injector-pulse-on and off. The operational densities were kept below  
76 this threshold to eliminate the impact of self-injection. Shown in Figure 2 are typical e-beam spectra for  
77 the zero-delay case.



78

79 Figure 2. a) Spectral profiles of magnetically dispersed e-beams and b) corresponding spectral lineouts.  
 80 The left panel of (a) and the black curve in (b) show the e-beam generated with the drive pulse only. The  
 81 other beams were generated with both drive and injector pulses with no delay between them.

82 We then tuned the delay between the laser pulses. First, we scanned with large time-steps (67 fs), longer  
 83 than the plasma period (35 fs for density  $1.3 \times 10^{19} \text{ cm}^{-3}$ ). Robust injection was observed in the range of  
 84 delays from -850 fs to +950 fs (total of 50 plasma periods) resulting in stable quasi-monoenergetic e-  
 85 beams with an average charge at least twice of the charge measured with the drive pulse only. Shown in  
 86 Figure 3a are the central energy and charge of these beams. Negative (positive) delay times correspond to  
 87 the injector (drive) pulse arriving first to the intersection, see Figure 1a (c). Based on the experimental  
 88 geometry, the spatio-temporal overlap of the drive and injector pulses, at which they form a beatwave,  
 89 and at which electrons can be injected via stochastic heating in the beatwave [22], is limited to (-200 fs;  
 90 200 fs) [see Supplementary]. Such injection in similar delay range was observed by Plateau et al. [40].  
 91 Injection outside of this range, observed in our experiment, should be therefore attributed to different  
 92 mechanisms. For negative delays it is wake-wake interference, for positive delays it is wake-wake  
 93 interference and ponderomotive drift.

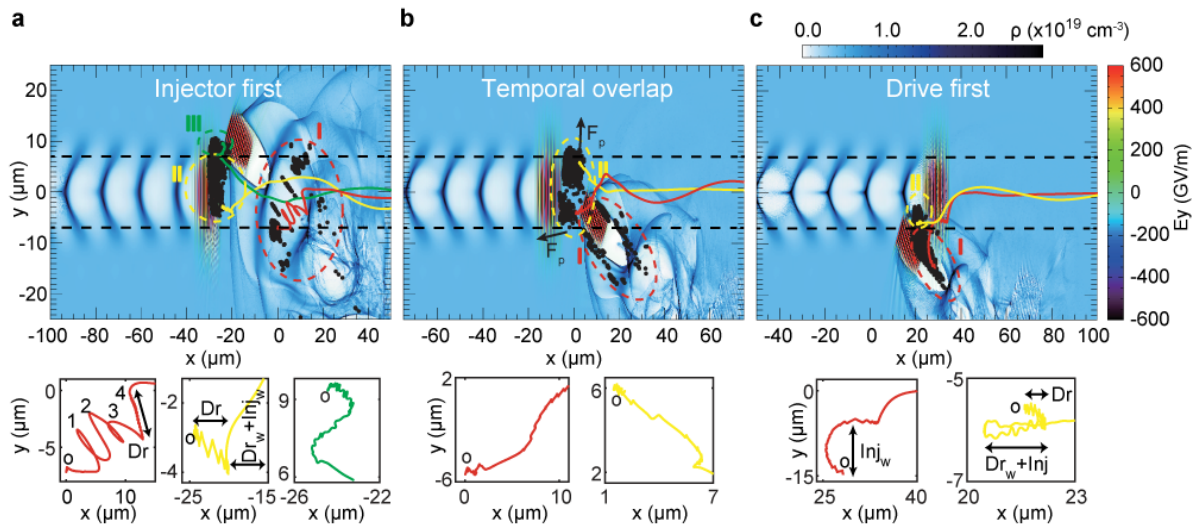


94

95 Figure 3. Electron-beam properties vs delay between the drive and injector laser pulses. a) Course time-  
 96 scan ( $n_e = 1.0 \times 10^{19} \text{ cm}^{-3}$ , plasma period  $\tau_p = 35$  fs). Each point shows 3.4 shots on average; the errorbars  
 97 show standard deviations. The green line shows results of PIC-simulations. Purple area shows charge  
 98 measured with the drive pulse only ( $\pm 1$  standard deviation). b) Fine time-scan ( $n_e = 7.6 \times 10^{18} \text{ cm}^{-3}$ ,  
 99  $\tau_p = 40$  fs). Each point shows 10 shots on average. Light blue area represents standard deviation of the  
 100 data, dark blue area – standard error of the mean. The red dashed lines show data fits with a) bi-Gaussian  
 101 function (red numbers show half-widths-at-half-maximum calculated from the fit); b) sums of sine and  
 102 linear functions (red number shows a period of the plasma wave, calculated from the fit).

103 To more precisely control position within the wakefield period at which the electrons were injected, we  
 104 tuned the delay between the laser pulses with a time-step of 6 fs, much smaller than the plasma period (40  
 105 fs at  $n_e = 7.6 \times 10^{18} \text{ cm}^{-3}$ ). The energy and charge of quasi-monoenergetic e-beams, measured during this  
 106 scan, are shown in Figure 3b. Both quantities exhibit oscillations, with a period ( $41 \pm 2$  fs, based on a sine  
 107 fit, red lines) that closely matches the plasma period. The same oscillations were seen when the delay was  
 108 scanned at twice-higher plasma density; however, the period decreased to  $31 \pm 5$  fs, consistent with the  
 109 plasma period (31 fs for  $1.3 \times 10^{19} \text{ cm}^{-3}$ ) [see Supplementary for additional experimental and numerical  
 110 modeling data]. Similar oscillations were observed in experiments on coupling of multiple laser-  
 111 wakefield-acceleration stages [41]. They result from electrons being injected in different phases of the

112 wakefield. The obvious anti-correlation of charge and energy of the e-beams (Figure 3a and b) can be  
 113 attributed to beam-loading [42]. The deviation from this pattern can be seen in the coarse scan in the  
 114 range of (-250 fs; 0 fs). It can be explained by a complex host of interactions of the laser pulses and  
 115 wakes. In particular, in the injector-pulse-first scenario, electrons pre-accelerated by the ponderomotive  
 116 force of the injector pulse and its wake and trapped in the drive wake might go through a decelerating  
 117 phase of the drive wake first and lose some energy, while in the drive-pulse-first scenario they are trapped  
 118 into an accelerating phase immediately (compare Figure 4a and c). It should be noted that the trends of  
 119 energy and charge on the coarse and fine-time scans can differ because they correspond to different time-  
 120 scales (10's of plasma periods for the coarse scan and only a few plasma periods for the fine one). Also,  
 121 the scans were done at slightly different plasma densities, which translated in different dynamics of the  
 122 laser pulses and their wakes, as well as the magnitude of beam-loading.



123  
 124 Figure 4. Results of PIC-simulations for electron injection into the drive wake in the cases when the  
 125 injector pulse arrives at the intersection before the driver pulse (a), at the same time (b), or after the driver  
 126 pulse (c). The white-blue-black (horizontal) color bar represents background plasma density, the red-  
 127 green-black (vertical) color bar – electric field. The black points are the initial positions of typical injected  
 128 electrons. The color curves show typical trajectories of those electrons. The figures at the bottom of each  
 129 panel show the same trajectories with “o” marking their starting points. “Dr,” “In,” “Dr<sub>w</sub>,” and “Inj<sub>w</sub>”  
 130 labels stand for drive pulse, injector pulse, drive wake, and injector wake respectively, and point to the  
 131 locations along electron trajectories experiencing the field of each.

132 To better understand the underlying physics of the injection process, we conducted two-dimensional  
 133 Particle-In-Cell (PIC) simulations with the code OSIRIS [43] (see Supplementary for details). While the  
 134 simulations showed injection into both drive and injector wakes, for the purposes of this paper we focused

135 only on electrons injected in the drive wake. When the injector pulse arrives first (Figure 4a), three groups  
136 of electrons are injected. Electrons from group I originate off-axis with respect to both pulses, so they do  
137 not experience their fields directly; instead, the injector wake dominates their motion. A representative  
138 particle trajectory is shown with the red curve. The high-frequency small-amplitude oscillations are due to  
139 direct laser acceleration at the drive-laser-pulse carrier frequency. The lower frequency high-amplitude  
140 oscillations are due to the interaction with the injector wake. These electrons are injected via wake-wake  
141 interference mechanism. Electrons in group II originate directly on the axis of the drive pulse, and to the  
142 side of the injector pulse (yellow trajectory). These electrons first experience the interaction with the drive  
143 pulse, and then kicked and injected into the drive wakefield by the combination of the injector pulse's  
144 ponderomotive force and its wakefield [19,44,45]. This group is injected via ponderomotive drift and,  
145 partially, due to stochastic heating in the beatwave. Electrons in group III originate in front of the injector  
146 pulse (green trajectory), they experience both injector and drive pulses, as well as the fields of their  
147 wakefields [30].

148 When the drive and injector pulses overlap, electrons from groups I and II are injected (Figure 4b).  
149 Electrons from group II receive strong forward or backward kick (depending on their transverse positions)  
150 from the ponderomotive force of the injector pulse, which traps them into the drive wake. When the drive  
151 pulse arrives first, most charge originates from group I (Figure 4c). Those electrons are initially located  
152 on the right side of the injector pulse and experience its wakefield, which kicks them into the drive wake.  
153 Small perturbations due to interaction with injector (near the beginning) and drive (near the center) pulses  
154 can be seen on the trajectories. Electrons from group II are also located on the right side of the injector  
155 pulse, but closer to its axis.

156 The amount of injected charge as a function of time delay is shown in Figure 3a. Simulation results (green  
157 line) match well the experimental trends: the charge drops faster for the drive-pulse-first scenario than for  
158 the injector-pulse-first one. This asymmetry is clearly seen in the bi-Gaussian fit of the experimental data  
159 (red dashed line): the half-width-at-half-maximum is  $180 \pm 20$  fs for the drive-pulse-first case and  $500 \pm 50$   
160 fs for the injector-pulse-first case. It can be attributed mainly to the intensity difference between the  
161 pulses. In the drive-pulse-first case, the injector's wake dominates electron trajectories at the intersection.  
162 As a result, electron acceleration along the drive-pulse direction is suppressed, and total injected charge  
163 drops quickly with increasing delay. In the injector-pulse-first case, the drive pulse collides with the  
164 injector wake, which exists for longer than the drive wake, since the injector pulse is much stronger than  
165 the drive one. Electrons oscillating in the injector wake have sufficient energy to be trapped into the drive  
166 wake for long times ( $10$ 's of plasma periods).



167 In the above simulations, the polarization planes of the drive and injector pulses were parallel to each  
168 other, as they were in the experiment. To study the impact of beatwave injection, we also performed a  
169 simulation with perpendicular polarizations, in which case the beatwave should not exist (see  
170 Supplementary). The total injected charge dropped by 24% at zero delay, as compared with the parallel-  
171 polarization case, indicating that beatwave injection was not dominant, even when the drive and injector  
172 pulses overlapped.

173 In summary, we discussed the results of a laboratory study of wave-wave interactions in plasma. The  
174 results experimentally confirmed long-standing, but previously untested, theories of electron injection via  
175 ponderomotive drift and wake-wake interference [19,30,31]. These mechanisms are shown to produce  
176 high-quality e-beams, which can be further improved by optimizing the driver-injector interaction  
177 geometry. Most importantly, precise control over the phase of the wake, at which injection takes place, is  
178 demonstrated. Such control has the potential to minimize energy spread and emittance, or increase charge,  
179 of wakefield-accelerated beams [46], whether laser-driven or charged-particle-driven [20,47]. These  
180 mechanisms also have an advantage of being relatively immune to laser timing jitter and amplitude  
181 fluctuation. The accelerated electrons can reveal features of strongly nonlinear wakes that are  
182 complementary to other plasma-wave diagnostic methods used to probe linear wakes, such as ultrafast  
183 shadowgraphy [48], holography [49,50], ultrafast polarimetry [51,52], and e-beam probes [53]. We  
184 believe this new diagnostic might eventually yield further insights into nonlinear plasma phenomena,  
185 such as energy transfer with highly non-linear plasma wakes, of interest in high-energy-density physics,  
186 astrophysics, and fusion plasmas.

187 This work was supported by National Science Foundation under Grant No. PHY-1535700 (ultra-low  
188 emittance electron beams), the US Department of Energy (DOE), Office of Science, Basic Energy  
189 Sciences (BES), under Award # DE-FG02-05ER15663 (laser-driven x-rays for ultrafast science), and the  
190 Air Force Office for Scientific Research under award number FA9550-14-1-0345 (interactions of  
191 electrons with laser light at highly relativistic intensities). This support does not constitute an express or  
192 implied endorsement on the part of the Government. We acknowledge technical assistance from Kevin  
193 Brown, Chad Peterson, Jun Zhang, and Bradley Nordell. MC acknowledges the support by the National  
194 Basic Research Program of China (Grant No. 2013CBA01504) and the NSFC (Grants No. 11774227,  
195 11721091). We also acknowledge the OSIRIS Consortium, consisting of UCLA and IST (Lisbon,  
196 Portugal) for the use of OSIRIS and the visXD framework. Simulations were performed on the  
197  $\Pi$  supercomputer at SJTU.

## 198 **References**

- 199 [1] J. M. Laming, *Astrophys. J.* **546**, 1149 (2001).
- 200 [2] Z. Fan, S. Liu, and C. L. Fryer, *Monthly Notices of the Royal Astronomical Society* **406**, 1337 (2010).
- 201 [3] R. Kirkwood, J. Moody, J. Kline, E. Dewald, S. Glenzer, L. Divol, P. Michel, D. Hinkel, R. Berger, and E.  
202 Williams, *Plasma Phys. Controlled Fusion* **55**, 103001 (2013).
- 203 [4] A. I. Akhiezer and R. Polovin, *Soviet Phys.JETP* **3** (1956).
- 204 [5] T. Tajima and J. Dawson, *Phys. Rev. Lett.* **43**, 267 (1979).
- 205 [6] E. Esarey, C. Schroeder, and W. Leemans, *Reviews of Modern Physics* **81**, 1229 (2009).
- 206 [7] V. Malka, *Phys Plasmas* **19** (2012).
- 207 [8] A. Rousse, K. T. Phuoc, R. Shah, A. Pukhov, E. Lefebvre, V. Malka, S. Kiselev, F. Burgy, J. P. Rousseau,  
208 D. Umstadter, *et al*, *Phys. Rev. Lett.* **93** (2004).
- 209 [9] F. Albert and A. G. Thomas, *Plasma Phys. Controlled Fusion* **58**, 103001 (2016).
- 210 [10] W. Leemans, A. Gonsalves, H. Mao, K. Nakamura, C. Benedetti, C. Schroeder, C. Tóth, J. Daniels, D.  
211 Mittelberger, and S. Bulanov, *Phys. Rev. Lett.* **113**, 245002 (2014).
- 212 [11] C. Joshi, *Physics of Plasmas* **14**, 055501 (2007).
- 213 [12] A. Modena, Z. Najmudin, A. E. Dangor, C. E. Clayton, K. A. Marsh, C. Joshi, V. Malka, C. B. Darrow, C.  
214 Danson, D. Neely, *et al*, *Nature* **377**, 606 (1995).

215 [13] S. Banerjee, S. Y. Kalmykov, N. D. Powers, G. Golovin, V. Ramanathan, N. J. Cunningham, K. J. Brown,  
216 S. Chen, I. Ghebregziabher, and B. A. Shadwick, Physical Review Special Topics-Accelerators and Beams  
217 **16**, 031302 (2013).

218 [14] S. Bulanov, N. Naumova, F. Pegoraro, and J. Sakai, Phys Rev E. **58**, R5257 (1998).

219 [15] S. Kalmykov, S. A. Yi, V. Khudik, and G. Shvets, Physical Review Letters **103**, 135004 (2009).

220 [16] J. Faure, C. Rechatin, O. Lundh, L. Ammoura, and V. Malka, Phys. Plasmas **17** (2010).

221 [17] A. Pak, K. A. Marsh, S. F. Martins, W. Lu, W. B. Mori, and C. Joshi, Phys. Rev. Lett. **104**, 025003  
222 (2010).

223 [18] C. McGuffey, A. G. R. Thomas, W. Schumaker, T. Matsuoka, V. Chvykov, F. J. Dollar, G. Kalintchenko,  
224 V. Yanovsky, A. Maksimchuk, K. Krushelnick, *et al*, Phys. Rev. Lett. **104**, 025004 (2010).

225 [19] D. Umstadter, J. K. Kim, and E. Dodd, Phys. Rev. Lett. **76**, 2073 (1996).

226 [20] B. Hidding, G. Pretzler, J. Rosenzweig, T. Königstein, D. Schiller, and D. Bruhwiler, Phys. Rev. Lett.  
227 **108**, 035001 (2012).

228 [21] M. Chen, E. Esarey, C. G. R. Geddes, E. Cormier-Michel, C. B. Schroeder, S. S. Bulanov, C. Benedetti,  
229 L. L. Yu, S. Rykovanov, D. L. Bruhwiler, *et al*, Physical Review Special Topics - Accelerators and Beams **17**,  
230 051303 (2014).

231 [22] E. Esarey, R. F. Hubbard, W. P. Leemans, A. Ting, and P. Sprangle, Phys. Rev. Lett. **79**, 2682 (1997).

232 [23] J. Faure, C. Rechatin, A. Norlin, A. Lifschitz, Y. Glinec, and V. Malka, Nature **444**, 737 (2006).

233 [24] J. Faure, C. Rechatin, A. Norlin, F. Burgy, A. Tafzi, J. Rousseau, and V. Malka, Plasma Phys. Controlled  
234 Fusion **49**, B395 (2007).

235 [25] C. Rechatin, J. Faure, A. Ben-Ismaïl, J. Lim, R. Fitour, A. Specka, H. Videau, A. Tafzi, F. Burgy, and V.  
236 Malka, Phys. Rev. Lett. **102**, 164801 (2009).

237 [26] H. Kotaki, I. Daito, M. Kando, Y. Hayashi, K. Kawase, T. Kameshima, Y. Fukuda, T. Homma, J. Ma, L. -.  
238 Chen, *et al*, Phys. Rev. Lett. **103**, 4 (2009).

239 [27] S. Corde, K. T. Phuoc, R. Fitour, J. Faure, A. Tafzi, J. P. Goddet, V. Malka, and A. Rousse, Phys. Rev.  
240 Lett. **107** (2011).

241 [28] M. Hansson, B. Aurand, H. Ekerfelt, A. Persson, and O. Lundh, Nuclear Instruments and Methods in  
242 Physics Research Section A: Accelerators, Spectrometers, Detectors and Associated Equipment **829**, 99  
243 (2016).

244 [29] J. Wenz, K. Khrennikov, A. Döpp, M. Gilljohann, H. Ding, J. Goetzfried, S. Schindler, A. Buck, J. Xu,  
245 and M. Heigoldt, arXiv preprint arXiv:1804.05931 (2018).

246 [30] R. G. Hemker, K. C. Tzeng, W. B. Mori, C. E. Clayton, and T. Katsouleas, Physical Review E **57**, 5920  
247 (1998).

248 [31] J. R. Cary, R. Giaccone, C. Nieter, and D. Bruhwiler, Phys Plasmas **12**, 056704 (2005).

249 [32] G. Wittig, O. Karger, A. Knetsch, Y. Xi, A. Deng, J. Rosenzweig, D. Bruhwiler, J. Smith, G. Manahan,  
250 and Z. Sheng, Physical Review Special Topics-Accelerators and Beams **18**, 081304 (2015).

251 [33] C. Liu, S. Banerjee, J. Zhang, S. Chen, K. Brown, J. Mills, N. Powers, B. Zhao, G. Golovin, and I.  
252 Ghebregziabher, in *SPIE LASE* (International Society for Optics and Photonics, 2013), p. 859919.

253 [34] W. Yan, C. Fruhling, G. Golovin, D. Haden, J. Luo, P. Zhang, B. Zhao, J. Zhang, C. Liu, M. Chen, *et al*,  
254 *nature photonics* **11**, 514 (2017).

255 [35] C. Liu, J. Zhang, S. Chen, G. Golovin, S. Banerjee, B. Zhao, N. Powers, I. Ghebregziabher, and D.  
256 Umstadter, *Opt. Lett.* **39**, 80 (2014).

257 [36] B. Zhao, J. Zhang, S. Chen, C. Liu, G. Golovin, S. Banerjee, K. Brown, J. Mills, C. Petersen, and D.  
258 Umstadter, *Optics express* **22**, 26947 (2014).

259 [37] See Supplemental Material [url] for the details on the jet density profile and its measurement,  
260 which includes Ref. [38].

261 [38] G. Golovin, S. Banerjee, J. Zhang, S. Chen, C. Liu, B. Zhao, J. Mills, K. Brown, C. Petersen, and D.  
262 Umstadter, *Appl. Opt.* **54**, 3491 (2015).

263 [39] E. Dodd, J. Kim, and D. Umstadter, in *AIP Conference Proceedings* (AIP, 1997), p. 106.

264 [40] G. R. Plateau, C. G. R. Geddes, N. H. Matlis, E. Cormier-Michel, D. E. Mittelberger, K. Nakamura, C. B.  
265 Schroeder, E. Esarey, W. P. Leemans, S. H. Gold, *et al*, in , *11* (AIP Publishing, 2010), p. 180.

266 [41] S. Steinke, J. Van Tilborg, C. Benedetti, C. Geddes, C. Schroeder, J. Daniels, K. Swanson, A.  
267 Gonsalves, K. Nakamura, and N. Matlis, *Nature* **530**, 190 (2016).

268 [42] C. Rechatin, J. Faure, X. Davoine, O. Lundh, J. Lim, A. Ben-Ismaïl, F. Burgy, A. Tafzi, A. Lifschitz, E.  
269 Lefebvre, *et al*, *New J. Phys.* **12** (2010).

270 [43] R. A. Fonseca, L. O. Silva, F. S. Tsung, V. K. Decyk, W. Lu, C. Ren, W. B. Mori, S. Deng, S. Lee, T.  
271 Katsouleas, *et al*, *OSIRIS: A Three-Dimensional, Fully Relativistic Particle in Cell Code for Modeling Plasma*  
272 *Based Accelerators* (Springer Berlin Heidelberg, 2002), 2331, p. 342.

273 [44] E. S. Dodd, J. K. Kim, and D. Umstadter, *Phys. Rev. E* **70** (2004).

274 [45] V. Horný, V. Petržílka, O. Klimo, and M. Krůs, *Phys Plasmas* **24**, 103125 (2017).

275 [46] S. Y. Kalmykov, L. M. Gorbunov, P. Mora, and G. Shvets, *Physics of Plasmas* **13**, 113102 (2006).

276 [47] R. Assmann, R. Bingham, T. Bohl, C. Bracco, B. Buttenschön, A. Butterworth, A. Caldwell, S.  
277 Chattopadhyay, S. Cipiccia, and E. Feldbaumer, *Plasma Phys. Controlled Fusion* **56**, 084013 (2014).

278 [48] M. Schwab, A. Sävert, O. Jäckel, J. Polz, M. Schnell, T. Rinck, L. Veisz, M. Möller, P. Hansinger, and G.  
279 Paulus, *Appl. Phys. Lett.* **103**, 191118 (2013).

280 [49] N. H. Matlis, S. Reed, S. S. Bulanov, V. Chvykov, G. Kalintchenko, T. Matsuoka, P. Rousseau, V.  
281 Yanovsky, A. Maksimchuk, S. Kalmykov, *et al*, *Nat Phys* **2**, 749 (2006).

282 [50] P. Dong, S. A. Reed, S. A. Yi, S. Kalmykov, Z. Y. Li, G. Shvets, N. H. Matlis, C. McGuffey, S. S. Bulanov,  
283 V. Chvykov, *et al*, *New Journal of Physics* **12** (2010).

284 [51] A. Buck, M. Nicolai, K. Schmid, C. M. S. Sears, A. Savert, J. M. Mikhailova, F. Krausz, M. C. Kaluza, and  
285 L. Veisz, *Nat Phys* **7**, 543 (2011).

286 [52] A. Flacco, J. Vieira, A. Lifschitz, F. Sylla, S. Kahaly, M. Veltcheva, L. Silva, and V. Malka, *Nature Physics*  
287 **11**, 409 (2015).

288 [53] C. Zhang, J. Hua, Y. Wan, C. Pai, B. Guo, J. Zhang, Y. Ma, F. Li, Y. Wu, and H. Chu, Phys. Rev. Lett. **119**,  
289 064801 (2017).